Optimal State Reference Computation With Constrained MTPA Criterion for PM Motor Drives

Matthias Preindl, *Student Member, IEEE*, and Silverio Bolognani, *Member, IEEE*

***Abstract*—This research proposes a procedure that maps a PMSM torque request onto optimal state (current) references. Combining the procedure with a dynamic (current) controller yields a torque controller. The maximum torque per ampere (MTPA) criterion is used to minimize conduction and switching losses. This research extends the concept to field-weakening operation to obtain high efficiency at any machine speed. The resulting constrained MTPA criterion is formalized as an optimization problem. Since it is difficult to solve directly, the maximum and intersection torque subproblems are identified. An algorithm is obtained that maps a torque onto an optimal state reference, and it is sufficiently efficient for real-time implementation. This method is compatible with a variety of state (current) controllers with/without PWM, SPM and IPM machines with saliency and reverse saliency, and a variable dc-link voltage. The proposed procedure relies on a sufficiently accurate torque model that may not be provided using rated machine parameters. Thus, an approach to compute locally optimized machine parameters is proposed that takes magnetic saturation into account. The concept is developed on a software-in-the-loop platform and evaluated on an experimental test bench.**

***Index Terms*—Drive system, field weakening (FW), internal permanent magnet synchronous motor, maximum torque per ampere (MTPA), optimal control.**

I. Introduction

PM synchronous motor drives consist of a PM synchronous motor, inverter, and control system. They are designed to apply a reference torque to a drive shaft that can be generated locally, e.g., by a speed controller, or it can be communicated via field bus to control a larger system, e.g., a wind turbine or a traction system. A PMSM produces torque driving a current (control state) in the stator windings that is controlled by the terminal voltage (control input). The current vector that generates a given torque is not unique, and a control system can achieve secondary control goals besides actuating a torque. A typical setup uses the maximum torque per ampere (MTPA) tracking below rated speed [1]–[3]. This minimizes conduction and switching losses [4], [5], i.e., yields operation at high efficiency and is necessary to achieve the rated torque. To achieve high-speed operation, field weakening (FW) is used to limit the terminal voltage such that it does not exceed its rated value [1], [6], [7].

Manuscript received March 3, 2014; revised July 21, 2014; accepted August 19, 2014. Date of publication September 4, 2014; date of current version March 5, 2015. Recommended for publication by Associate Editor J. Olorunfemi.

The authors are with the Department of Industrial Engineering, University of Padova, 35131 Padova, Italy (e-mail: matthias.preindl@gmail.com; silverio.bolognani@dii.unipd.it).

Color versions of one or more of the figures in this paper are available online at http://ieeexplore.ieee.org.

Digital Object Identifier 10.1109/TPEL.2014.2354299

FW concepts can be classified into feedback and feedforward methods. Feedback methods use a feedback of the terminal voltage [8], [9]. They are widely used but have also potential issues that need to be addressed during design and implementation: 1) the transition between MTPA and FW operation needs to be smooth; 2) voltage feedback ensures feasibility at high speed; this does not necessarily imply operation with low current magnitude (low losses) when the reference torque is small; 3) a voltage loop is (typically) an outer loop that needs to be decoupled in dynamics, i.e., have a slower transient response, than the inner loop due to the cascade structure; 4) a voltage loop can yield an outer (e.g., speed) controller unstable if it drives the current vector beyond the MTPV trajectory; here, an increase of the current magnitude (along the isoflux trajectories) corresponds to a *decrease* of torque; and 5) voltage control tuning is demanding due to the nonlinear equations involved. These points are inherently avoided using feedforward methods [10], [11] that act instantaneously (no dynamics involved) on the expense of relying on the machine model. In fact, this latter approach is interesting for applications where the machine model is reasonably well known (or at least some operation points as shown later). This is the case for applications where it is worth investigating the real machine behavior to produce good models, e.g., in drive systems that are produced in large series (electric vehicles) or high-power applications (railway traction or wind power). Also, good models are typically already available if model-predictive current control [5], [12] is used.

Present feedforward methods are written for surface-mounted permanent magnet synchronous machines (SPM) [13] or interior-mounted permanent magnet synchronous machines (IPM) with $L_d \leq L_q$; use approximations to simplify the (nonlinear) equation set [13]–[15]; and/or use iterative methods [11], [13], [15], [16]. Moreover, no attempt has been made to "invert" the PMSM torque equation online for torque control; the existing method computes a reference vector from a q-current [17] or current magnitude [10], [11]. This research proposes an unified way to compute *optimal state references* from a torque reference at all machine speeds based on the feedforward idea. The MTPA concept is extended to speeds where field weakening is required introducing the constrained MTPA criterion. The problem is written as a constrained optimization problem, that minimizes the current magnitude taking the system constraints into account. The constrained MTPA criterion defines the optimal state vector that generates a desired, i.e., reference, torque. It is a static function that depends on a single operation parameter (normalized speed, i.e., is the machine speed divided by the rated terminal voltage). It results in a parameterized static function, which maps torque onto optimal states and can be

TABLE I
NOMENCLATURE

Symbol	Description
$\mathbf{1}$	Vector of ones
$.^{\dagger}$	Moore–Penrose pseudoinverse
$\|.\|$	Euclidean norm
$\circ$	Convolution
∂	Boundary of a set
$\oplus$ and $\ominus$	Minkowski sum and Pontryagin difference [18]
$\cap$ and $\cup$	Intersection and union of sets
$\mathbb{R}$ and $\mathbb{R}_+$	Real and nonnegative real numbers
$\emptyset$	Empty set
i_{dq} and λ_{dq}	Stator current and flux
v_{dq}	Terminal voltage
$\mathbf{L}$ and ψ_{dq}	Inductance matrix and PM flux
$\mathcal{I}$ and I_r	Set of feasible currents and rated current
Λ and $\bar{v}_r$	Set of feasible fluxes and rated voltage
T, T_m, T_i	Actual, maximum, and intersection torque
χ_r and χ_p	Normalized rated and rated power speed param.
χ_i and χ_m	Normalized intersection and max. speed param.

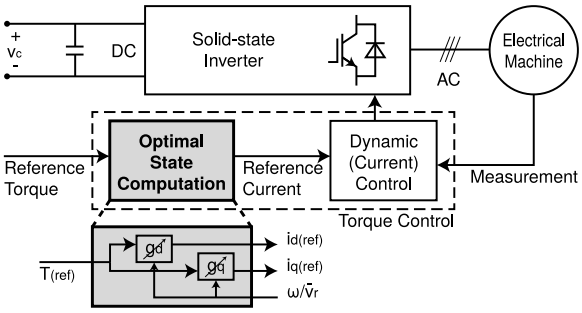

Fig. 1. Torque control block diagram: static reference generation procedure and a dynamic controller.

interpreted as a variable (nonlinear) gain that acts between the torque and state references as shown in Fig. 1. Combining the (static) state reference generation procedure with a (dynamic) current controller yields a (dynamic) torque controller as it is shown in Fig. 1. The transient behavior (the trajectory of the state to its reference) and transient constraint satisfaction of the resulting controller depends only on the current controller and is not analyzed in this text. Since torque feedback is not practicable in most applications due to cost and reliability issues, the resulting torque controller relies on a (optimized) machine model.

The constrained MTPA optimization problem is a nonconvex quadratically constrained quadratic program that is difficult to solve in general. Thus, it is divided into subproblems. The *maximum torque problem* defines whether a reference torque is feasible or not. The *intersection torque problem* yields information if the optimal operation happens on the MTPA or the isoflux trajectory. Each of these subproblems can be solved using the low dimensionality of the problem and system properties. The solution is obtained analytically intersecting the relevant trajectories [11], [19].

Relying on the machine model is a potential issue [20]–[22] and needs to be addressed when designing a feedforward method. In particular, saturation and cross saturation can be addressed using lookup tables [11]. However, flux or inductance planes may not be available for a machine and do prevent the (nonlinear) equation set from having a closed solution. Thus, a procedure is proposed to optimize the torque model locally with respect to important operation points, i.e., the rated operation point and the demagnetization or maximum speed operation point.

A variable dc-link voltage is interesting for many applications to minimize switching losses, i.e., increase efficiency [23], [24]. Thus, the method is written to be compatible with a (reasonably slow) varying dc link that is, e.g., obtained when the dc link is connected directly to a battery pack. The reference generation procedure is evaluated on a software-in-the-loop (SiL) platform, where the electrical machine is simulated by MATLAB/Simulink, and an experimental test bench. The algorithm is shown to be sufficiently efficient for online implementation, and key aspects of the algorithm are evaluated on these platforms. The nomenclature of this text is outlined in Table 1.

II. Electromagnetic Model

PMSM are typically described in the dq reference frame to simplify the treatment [25]. There, the dynamic of a three-phase neutral-point isolated armature winding is given by the state-space system [19]

$$\dot{\lambda}_{dq}(t) = -\omega(t)\mathbf{J}\lambda_{dq}(t) + v_{dq}(t) - R_s i_{dq}(t) \tag{1}$$

where $\lambda_{dq}(t) \in \mathbb{R}^2$ is the stator flux, $v_{dq}(t) \in \mathbb{R}^2$ is the terminal voltage, and $R_s i_{dq}(t)$ is the resistive voltage drop. The parameter $R_s \in \mathbb{R}_+$ is the resistance per phase, and $i_{dq}(t) \in \mathbb{R}^2$ is the phase current. The angular velocity $\omega(t) \in \mathbb{R}$ is the rotational velocity of the dq reference frame with respect to the stationary $\alpha\beta$ reference frame with respect to the transformation angle $\dot{\epsilon}(t) = \omega(t)$, and $\mathbf{J}$ is the rotation matrix $\mathbf{J} = [[0, -1]', [1, 0]']'$.

This system can be simplified introducing the *compensated voltage*

$$\bar{v}_{dq}(t) = v_{dq}(t) - R_s i_{dq}(t) \tag{2}$$

that yields the state-space system

$$\dot{\lambda}_{dq}(t) = -\omega(t)\mathbf{J}\lambda_{dq}(t) + \bar{v}_{dq}(t). \tag{3}$$

Changing the system input from $v_{dq}(t)$ to $\bar{v}_{dq}(t)$ means compensating the voltage drop $R_s i_{dq}(t)$ at each time instant with the terminal voltage $v_{dq}(t)$.

The flux-current dependence of a PMSM is a static nonlinear map, where the nonlinearity is introduced by saturation and cross saturation [26]–[28]. A nonlinear function $l : \mathbb{R}^2 \to \mathbb{R}^2$ is necessary to describe this relation in general but it yields a model, which is difficult to analyze. In most cases, the complexity is not justified since the local system behavior can be captured with good approximation (see Section VIII) by the linear function [29]–[31]

$$\lambda_{dq}(t) = l(i_{dq}(t)) \approx \mathbf{L} i_{dq}(t) + \psi_{dq} \tag{4}$$

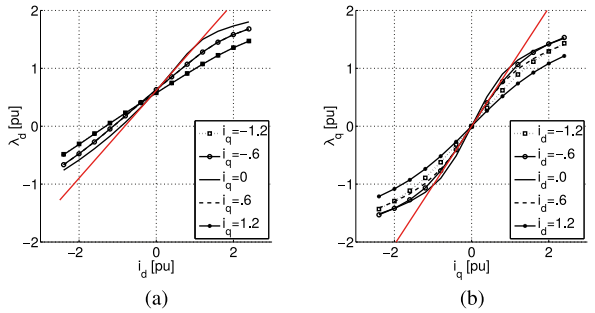

Fig. 2. Example of a measured nonlinear flux-current characteristic and the linear approximation using *rated* parameters. (a) d-axis. (b) q-axis.

that is characterized by the parameters

$$\mathbf{L} = \begin{bmatrix} L_d & 0 \\ 0 & L_q \end{bmatrix}, \quad \psi_{dq} = \begin{bmatrix} \psi \\ 0 \end{bmatrix} \tag{5}$$

where $L_d \in \mathbb{R}_+$ and $L_q \in \mathbb{R}_+$ are the autoinductance of the d- and q-axis, respectively and ψ_{dq}, i.e., $\psi \in \mathbb{R}_+$, is the flux generated by the PM. An example of the approximation is shown in Fig. 2.

Electric machines produce torque when currents are driven in armature winding (stator of a PMSM). There, the current interacts with the magnetic field, i.e., flux and produces the electromagnetic torque $T \in \mathbb{R}$ (with exception when the stator current and flux vector are parallel). The torque equation is obtained as power balance of the electromechanical energy conversion neglecting the resistive voltage drop and the angle dependent variation of the magnetic coenergy [31], [32]

$$T = \frac{3}{2} p i'_{dq} \mathbf{J} \boldsymbol{\lambda}_{dq} \tag{6}$$

where the parameter $p \in \mathbb{N}_+$ is the number of pole pairs of the electrical machine.

III. Constraints

An electric machine cannot be operated with arbitrarily large voltages and currents due to the finite terminal voltage that can be applied to the machine terminals (and supplied by an inverter) and thermal constraints. In this section, operation constraints are highlighted that have to be satisfied (at least) in steady-state conditions. Time dependences (t) are omitted for compactness.

The magnitude of the stator current needs to be limited since a winding is able to transmit only a finite amount of heat, i.e., power losses, to the ambient without exceeding its maximum operating temperature. Similarly, a high current magnitude leads to excessive thermal cycling of the solid-state valves of the inverter and their early failure. Thus, we obtain the *current constraint*

$$i_{dq} \in \mathcal{I} \stackrel{\text{def}}{=} \left\{ i_{dq} \in \mathbb{R}^2 \middle| \|i_{dq}\| \leq I_r \right\} \tag{7}$$

where $I_r \in \mathbb{R}_+$ is the rated current. The set $\mathcal{I}$ can be projected onto the flux space with $\bar{\mathcal{I}} \stackrel{\text{def}}{=} \mathbf{L} \circ \mathcal{I} + \psi_{dq}$.

A voltage source inverter can provide a terminal voltage with a finite maximum magnitude. A inverter can apply a voltage

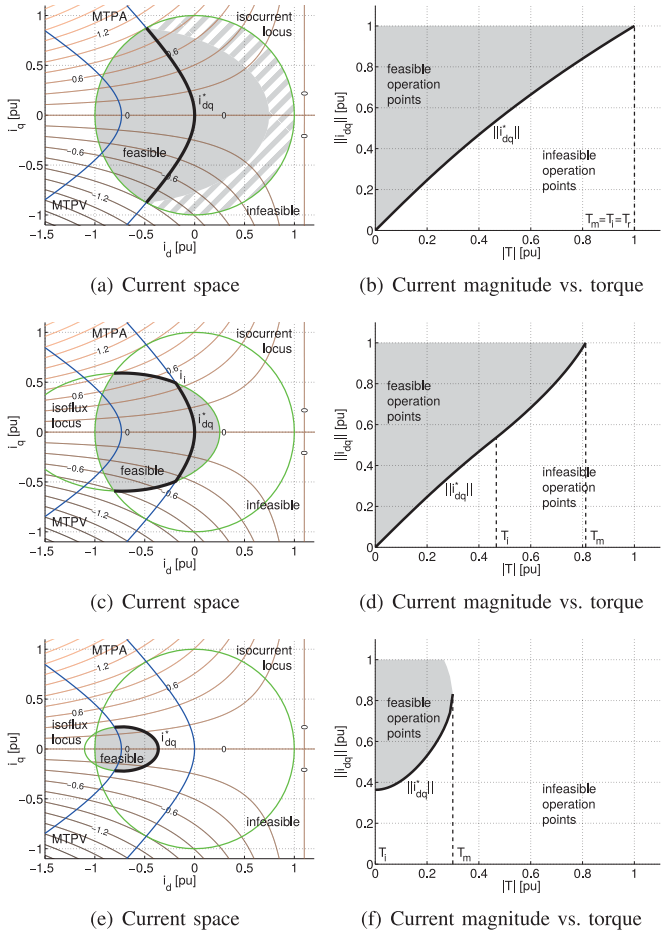

Fig. 3. Optimal operation; (a) and (b): base mode (constant torque mode); (c) and (d): field-weakening operation (constant power mode); (e) and (f): field-weakening operation (reduced power mode).

that lies within a set with hexagonal shape. However, this set is backward rotating in the dq system. Thus, the largest time-invariant approximation of the input set is used

$$v_{dq} \in \mathcal{V} \stackrel{\text{def}}{=} \left\{ v_{dq} \in \mathbb{R}^2 \middle| \|v_{dq}\| \leq v_r \right\} \tag{8}$$

where $v_r \in \mathbb{R}_+$ is the rated voltage. This set depends on the dc-link voltage $v_c \in \mathbb{R}_+$ and is defined by $v_r \stackrel{\text{def}}{=} v_c/\sqrt{3}$ for a two-level inverter. Throughout this research, it is assumed that the dc link, i.e., v_r, is not necessarily constant and may vary within certain bounds, e.g., due to voltage variations in the power grid or in a distributed dc-link system.

Using the compensated terminal voltage (2) as input, it must be ensured that $\bar{v}_{dq}$ can be applied to the system. In other words, the existence of a terminal voltage $v_{dq} \in \mathcal{V}$ for all $i_{dq} \in \mathcal{I}$ is required. Thus, the compensated terminal voltage has to satisfy the *voltage constraint*

$$\bar{v}_{dq} \in \mathcal{V} \ominus R_s \mathcal{I} = \left\{ \bar{v}_{dq} \in \mathbb{R}^2 \middle| \|\bar{v}_{dq}\| \leq v_r - R_s I_r \right\}. \tag{9}$$

Clearly, some of the available terminal voltage is lost above all if $\|i_{dq}\| \ll I_r$. However, this approach is justified for drive systems where the resistive voltage drop is small compared

to the rated voltage, i.e., $R_s I_r \ll v_r$. The compensated voltage approach can be generalized to take model uncertainties and nonlinear inverter behavior into account (dead times and forward voltage drop tend to decrease the maximum available voltage). A safety factor $\rho_v \in (0,1)$ is introduced to define rated compensated terminal voltage set

$$\bar{v}_{dq} \in \bar{\mathcal{V}} \stackrel{\text{def}}{=} \left\{ \bar{v}_{dq} \in \mathbb{R}^2 | \|\bar{v}_{dq}\| \leq \bar{v}_r \stackrel{\text{def}}{=} \rho_v v_r \right\}. \tag{10}$$

The factor ρ_v can be chosen heuristically such that $\bar{v}_r \leq v_r - R_s I_r$; typical values are $\rho_v = (0.8, 1)$. For applications, where generator operation is significant, it is possible to choose different safety factors (ρ_{v+} and ρ_{v-}) dependent on whether the mechanical power of the PMSM is positive or negative. Since ρ_{v-} (generator operation) can be selected larger ($\rho_{v-} > \rho_{v+}$), both the base speed and the maximum torque above base speed can be increased in generator operation. Throughout this paper, a single safety factor is used for simplicity.

In steady-state conditions, i.e., $\dot{\lambda}_{dq} = -\omega \mathbf{J} \lambda_{dq} + \bar{v}_{dq} = 0$, the input constraint maps onto a state constraint. In other words, a state can be maintained by the system if and only if $\omega \mathbf{J} \lambda_{dq} \in \bar{\mathcal{V}}$. Since $\mathbf{J}^{-1} \circ \bar{\mathcal{V}} = \bar{\mathcal{V}}$, the steady-state constraint becomes $\omega \lambda_{dq} \in \bar{\mathcal{V}}$ or

$$\lambda_{dq} \in \Lambda \stackrel{\text{def}}{=} \left\{ \lambda_{dq} \in \mathbb{R}^2 | |\omega| \|\lambda_{dq}\| \leq \bar{v}_r \right\}. \tag{11}$$

The set Λ can be projected onto the current space with $\bar{\Lambda} \stackrel{\text{def}}{=} \mathbf{L}^{-1} \circ (\Lambda - \psi_{dq})$.

The constraints (7) and (11) also define the high-speed behavior of a PMSM. The location of the current and voltage constraint with respect to each other defines whether a machine has an electrically limited maximum speed or not [1]. The center of $\bar{\Lambda}$ is the so-called demagnetization current $i_c \stackrel{\text{def}}{=} [-\psi/Ld, 0]'$. If $i_c \notin \mathcal{I}$, the PMSM has a limited maximum speed ω_m since $\mathcal{I} \cap \bar{\Lambda} = \emptyset$ for $|\omega| \to \infty$. Contrarily, a PMSM with $i_c \in \mathcal{I}$ has the maximum speed $\omega_m = \infty$ since there exists a current vector (i_c) that satisfies the system constraints for all $\omega \in \mathbb{R}$. Thus, a PMSM is subject to the *speed constraint*

$$\frac{|\omega|}{\bar{v}_r} \leq \chi_m \stackrel{\text{def}}{=} \begin{cases} \frac{1}{|\psi - L_d I_r|}, & \text{if } \frac{\psi}{L_d} > I_r \\ \infty, & \text{otherwise.} \end{cases} \tag{12}$$

where χ_m is the maximum speed normalized by the voltage $\bar{v}_r$. This approach is convenient since the maximum speed $\omega_m = \bar{v}_r / |\psi - L_d I_r|$ of a machine varies with $\bar{v}_r$. On the other hand, whether a machine has a maximum speed or not is independent of $\bar{v}_r$. Machines with $\chi_m = \infty$ and $\chi_m < \infty$ are depicted in Fig. 4.

It can be shown that any state reference, which satisfies the constraints outlined in this section, can be reached by a controller [19]. However, if a specific controller does converge to a reference is a current control property that needs to be verified when designing and implementing the controller.

IV. Optimal Operation

An electrical machine is designed to apply an electromagnetic torque to the drive shaft. However, the current, i.e., flux,

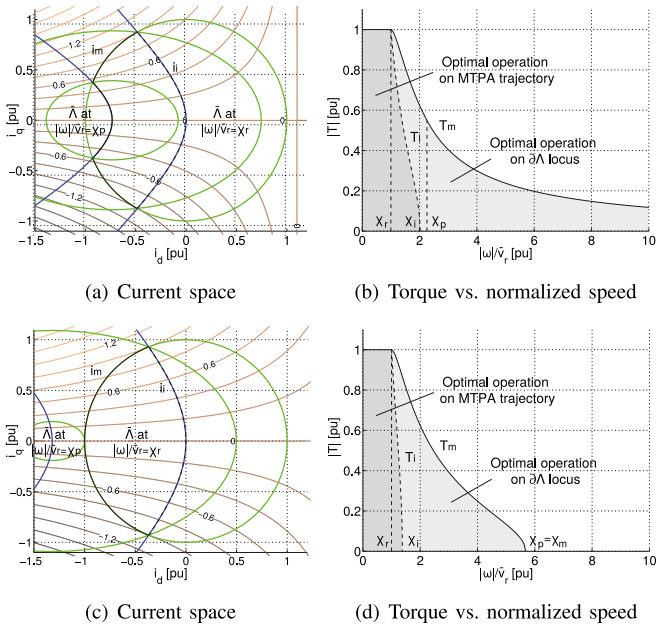

(a) Current space (b) Torque vs. normalized speed

(c) Current space (d) Torque vs. normalized speed

Fig. 4. Maximum and intersection torque characteristic ($L_d < L_q$); (a) and (b): infinite maximum speed $\chi_m = \infty$; (c) and (d): finite maximum speed $\chi_m < \infty$.

which produces a desired torque T, is not unique in general and provides an additional degree of freedom. The available degree of freedom can be exploited to increase the drive system efficiency. The drive system efficiency is typically maximized by minimizing the resistive losses, i.e., the current magnitude [1], [3], [7], [33]. Thus, the operation is said to be *optimal*, if a torque T is generated by the current $i^\star_{dq}$ and flux $\lambda^\star_{dq}$ that solve

$$\underset{i_{dq}, \lambda_{dq}}{\text{minimize}} \quad \|i_{dq}\| \tag{13a}$$

$$\text{subject to} \quad \|i_{dq}\| \leq I_r \tag{13b}$$

$$|\omega| \|\lambda_{dq}\| \leq \bar{v}_r \tag{13c}$$

$$\lambda_{dq} = \mathbf{L} i_{dq} + \psi_{dq} \tag{13d}$$

$$3/2 p i'_{dq} \mathbf{J} \lambda_{dq} = T \tag{13e}$$

$$|T| \leq T_m(\omega, \bar{v}_r). \tag{13f}$$

This constrained optimization problem uses the current magnitude (13a) as an objective function, which should be minimized. The current $i_{dq} \in \mathcal{I}$ (13b) and flux $\lambda_{dq} \in \Lambda$ (13c) constraint needs to be considered when solving for the optimal states. The relation between currents and fluxes is defined by (13d). The constraint (13e) defines the desired torque T, which is a parameter that has to satisfy the (speed-dependent) maximum torque $T_m(\omega, \bar{v}_r)$ constraint (13f).

The problem (13) is nonconvex due to the nonlinear equality constraint (13e). Thus, it is NP hard to solve in general [34] and can be infeasible dependent on the parameters. Thus, it is advantageous to break (13) down into subproblems that can be solved exploiting the low dimensionality and system properties.

In the next sections, an approach is proposed that computes a solution using the characteristic trajectories and loci of PMSM,

in particular: the MTPA trajectory [3]; the maximum torque per volt (MTPV) trajectory [7]; the isoflux locus $\partial\Lambda$ (boundary of Λ); and the isocurrent locus $\partial\mathcal{I}$ (boundary of $\mathcal{I}$). Examples of optimal operation in base mode (constant torque mode), field-weakening constant and reduced (apparent) power mode are shown in Fig. 3.

V. Maximum Torque

Prior to solving for optimal states given a desired torque, it must be ensured that (13) has a solution. Since state and input constraints apply to the PMSM, the maximum (and minimum) available torque is limited as well. In this section, an approach to find the maximum (steady state) torque $T_m \in \mathbb{R}_+$, which can be provided by the PMSM, is shown. For compactness, the dependences $(\omega, \bar{v}_r)$ are omitted. Due to the symmetries of the torque equation and constraints, finding T_m is equivalent to finding the minimum torque, which is the additive inverse of T_m, i.e., $-T_m$. Thus, the maximum torque is defined to be

$$T_m \stackrel{\text{def}}{=} \frac{3}{2}p \qquad \max_{i_{dq},\lambda_{dq}} \quad i'_{dq}\mathbf{J}\lambda_{dq} \tag{14a}$$

$$\text{subject to} \quad \|i_{dq}\| \le I_r \tag{14b}$$

$$|\omega|\|\lambda_{dq}\| \le \bar{v}_r \tag{14c}$$

$$\lambda_{dq} = \mathbf{L}i_{dq} + \psi_{dq}. \tag{14d}$$

The problem uses the torque equation (14a) as an objective function, which should be maximized. The steady-state current (14b) and voltage (14c) limit define the set where the current, i.e., fluxes, can lie. Due to the $|\omega|$ dependence of the voltage limit (14c), the maximum torque T_m depends on the machine speed and the rated voltage. The linear equality constraint (14d) defines the relation of currents and fluxes. The problem (14) can be written as a quadratic constrained quadratic program (qcqp) in standard form. However, the cost function is indefinite. Thus, rather than solving the problem directly, a solution is proposed using the low dimensionality and system properties. Examples of the maximum torque are shown in Fig. 4.

At low velocities ($\omega \approx 0$), the machine is said to work in *base mode* or *constant torque mode* [1], [3], [33]. There, the voltage constraint (14c) is always true. The torque T_m is produced by the current $i_m \in \mathbb{R}^2$, which lies on the MTPA trajectory, which is denoted as $i_m \in$ MTPA. Moreover, i_m lies on the largest admissible isocurrent locus, i.e., the border of $\mathcal{I}$, $i_m \in \partial\mathcal{I}$. The intersection MTPA $\cap\, \partial\mathcal{I}$ defines a set containing two current vectors, which produces the maximum and minimum torque. The solution $i_q > 0$ is named *rated* operation point, where the machine uses the rated current $i_r \in \mathbb{R}^2$, i.e., rated flux $\lambda_r \stackrel{\text{def}}{=} \mathbf{L}i_r + \psi_{dq}$, to produce the rated torque $T_r \stackrel{\text{def}}{=} 3/2pi'_r\mathbf{J}\lambda_r$. The maximum torque $T_m = T_r$ can be achieved iff $\lambda_r \in \Lambda$. Since Λ shrinks with increasing $|\omega|$, the machine works in constant torque mode if

$$\frac{|\omega|}{\bar{v}_r} \le \chi_r \stackrel{\text{def}}{=} \frac{1}{\|\lambda_r\|} \tag{15}$$

where χ_r is the rated speed $\omega_r = \bar{v}_r/\|\lambda_r\|$ normalized by the voltage $\bar{v}_r$. This approach is convenient since ω_r and the rated power $P_r = T_r\omega_r$ of a drive system vary with $\bar{v}_r$.

The PMSM is said to work in *field weakening*, if the speed is higher than the rated one ($|\omega|/\bar{v}_r > \chi_r$) [1], [7], [35], [36]. In this condition, the rated flux $\lambda_r \notin \Lambda$ cannot be achieved, and the updated maximum torque $T_m < T_r$ must be found. Considering the positive half-plane ($i_q \ge 0$, $\lambda_q \ge 0$), the torque increases along the largest isoflux locus $\partial\Lambda$ starting at the d-axis until its peak is achieved when intersecting the MTPV trajectory. Consequently, T_m is obtained at the intersection MTPV $\cap\, \partial\Lambda$ if this point satisfies $i_{dq} \in \mathcal{I}$. Otherwise, T_m is obtained at the intersection $i_{dq} \in \partial\mathcal{I}$ with $\lambda_{dq} \in \partial\Lambda$.

To simplify the treatment, the *rated power* operation point is introduced, which defines the current i_p and the flux $\lambda_p \stackrel{\text{def}}{=} \mathbf{L}i_p + \psi_{dq}$. It is defined to be the intersection of the MTPV trajectory with the isocurrent locus $\partial\mathcal{I}$, if it exists. It does exist for machines with $\chi_m = \infty$, which is shown in Fig. 4(a). Otherwise MTPV $\cap\, \partial\mathcal{I} = \emptyset$ and the rated power operation point is defined to be $i_p = [-I_r, 0]'$, which is shown in Fig. 4(c).

If $\lambda_p \in \Lambda$ (and $\lambda_r \notin \Lambda$), the machine is said to work in *constant (apparent) power mode* [1], [7]. In this mode, the maximum torque T_m is obtained at the intersection of $i_{dq} \in \partial\mathcal{I}$ with $\lambda_{dq} \in \partial\Lambda$. Similar to the constant torque mode, the machine works in constant power mode if

$$\chi_r < \frac{|\omega|}{\bar{v}_r} \le \chi_p \stackrel{\text{def}}{=} \frac{1}{\|\lambda_p\|} \tag{16}$$

where χ_p is the rated power speed $\omega_p = \bar{v}_r/\|\lambda_p\|$ normalized with the voltage $\bar{v}_r$.

Machines with electrically limited maximum speed $\chi_m < \infty$ cannot exceed the constant power mode, since $\chi_p \equiv \chi_m$. On the other hand, machines with $\chi_m = \infty$ can achieve $|\omega|/\bar{v}_r > \chi_p$, which is named *reduced (apparent) power mode* [1], [3], [7], [33]. In reduced power mode, the intersection MTPV $\cap\, \partial\Lambda$ satisfies $i_{dq} \in \mathcal{I}$ and defines therefore the current, i.e., flux, which provides T_m. The maximum torque T_m characteristic is shown in Fig. 4 for machines with $\chi_m = \infty$ and $\chi_m < \infty$.

VI. Intersection Torque

After ensuring that a desired torque value T is feasible $|T| \le T_m$, the optimal operation points can be computed. The optimal operation point $\|i^\star_{dq}\|$, i.e., $\|\lambda^\star_{dq}\|$, are computed by minimizing the current magnitude. This approach leads to two cases: operation on the MTPA trajectory or operation on $\partial\Lambda$ locus. To distinguish the two cases, the intersection torque $T_i \in \mathbb{R}_+$ is introduced

$$T_i \stackrel{\text{def}}{=} \frac{3}{2}p \qquad \max_{i_{dq},\lambda_{dq}} \quad i'_{dq}\mathbf{J}\lambda_{dq} \tag{17a}$$

$$\text{subject to} \quad \|i_{dq}\| \le I_r \tag{17b}$$

$$|\omega|\|\lambda_{dq}\| \le \bar{v}_r \tag{17c}$$

$$\lambda_{dq} = \mathbf{L}i_{dq} + \psi_{dq} \tag{17d}$$

$$i_{dq} \in \text{MTPA}. \tag{17e}$$

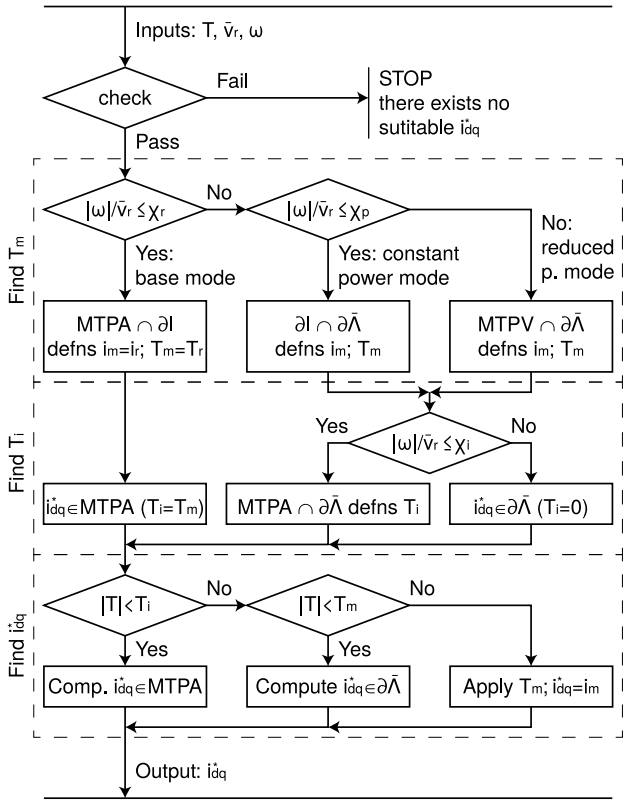

Fig. 5. Flux diagram of the reference generation procedure.

Theproblem (17) corresponds to problem (14) adding the constraint (17e) that requires the state to lie on the MTPA trajectory. Therefore, (17) is more restrictive than (14) such that $T_i \le T_m$.

Moreover, the problem (17) has a solution if and only if MTPA $\cap\, \partial\bar{\Lambda} \neq \emptyset$ that is achieved when $0 \in \bar{\Lambda}$ and yields the condition

$$\frac{|\omega|}{\bar{v}_r} \le \chi_i \stackrel{\text{def}}{=} \frac{1}{\psi}. \tag{18}$$

Otherwise, no MTPA operation point is available, and the intersection torque is defined to be $T_i = 0$. Examples of the intersection torque are shown in Fig. 4.

In base mode, the maximum torque T_r is achieved on the MTPA trajectory and corresponds therefore with the intersection torque $T_i = T_m$. Thus, the PMSM is operated exclusively on the MTPA trajectory if $|\omega|/\bar{v}_r \le \chi_r$. This behavior is expected since per definition, the MTPA states are the ones with minimum current magnitude and can produce any torque $|T| \le T_m$ in base mode. This operation is shown in Fig. 3(a) and (b).

In field weakening ($|\omega|/\bar{v}_r > \chi_r$), the maximum torque T_m is produced by states off the MTPA trajectory and as a consequence $T_i < T_m$. In this case, the intersection torque defines if a desired torque can be produced by a state that lies on the MTPA trajectory. If $T \le T_i$, then this is possible, i.e., $i_{dq}^{\star} \in$ MTPA; otherwise $i_{dq}^{\star} \in \partial\bar{\Lambda}$. This operation is shown in Fig. 3(c) and (d). At high speeds ($|\omega|/\bar{v}_r > \chi_i$), $\bar{\Lambda}$ does not contain states of the MTPA trajectory and MTPA $\cap\, \partial\Lambda = \emptyset$. Thus, the operation happens exclusively on the $\bar{\Lambda}$ locus, i.e., $i_{dq}^{\star} \in \partial\bar{\Lambda}$ and is achieved setting $T_i = 0$. This operation is shown in Fig. 3(e) and (f).

VII. Reference Generation Procedure

In this section, a state reference generation procedure is outlined based on the concepts introduced in the former sections. This procedure defines an efficient approach to compute the optimal current reference vector $i_{dq}^{\star}$ from a desired torque reference value T and the parameters $\bar{v}_r$ and ω. The obtained vector $i_{dq}^{\star}$ can then be used as reference for a dynamic controller.

The reference generation is carried out in four steps and is described by the block diagram in Fig. 5. The first step is to check the measurements to ensure that there exists a suitable reference $i_{dq}^{\star}$. The dc-link voltage is required to be positive $\bar{v}_r \ge 0$, and $|\omega|/\bar{v}_r$ is required to not exceed the maximum normalized velocity χ_m of the machine. Otherwise, $\Lambda = \emptyset$ or $\mathcal{I} \cap \bar{\Lambda} = \emptyset$ and no $i_{dq}^{\star} \in \bar{\Lambda}$ satisfying the constraints exists. Contrarily, operation is allowed if the desired torque exceeds the maximum torque $|T| > T_m$. In this case, it is assumed that the drive system should apply the largest available torque value $\pm T_m$.

The second step is identifying the operation mode (constant torque mode, constant power mode, reduced power mode) and computing the maximum torque T_m. The rated operation point λ_r (and i_r, T_r) and rated power operation point λ_p are parameters of the PMSM and can be computed offline. If $|\omega|/\bar{v}_r \le \chi_r$, the drive system works in base mode (constant torque mode), and the maximum torque is $T_m = T_r$ (generated by $i_m = i_r$). Otherwise, the drive system works in field weakening and the maximum torque depends on ω and $\bar{v}_r$. If $\chi_r < |\omega|/\bar{v}_r \le \chi_p$, the drive system works in constant power mode, and the maximum torque T_m is obtained at $i_m \in \partial\bar{\Lambda} \cap \partial\mathcal{I}$ (with $i_q > 0$). If $|\omega|/\bar{v}_r > \chi_p$, the drive system works in field weakening (reduced power mode), and the maximum torque T_m is obtained at $i_m \in$ MTPV $\cap\, \partial\bar{\Lambda}$ (with $i_q > 0$).

The third step is identifying whether optimal operation is achieved on the MTPA trajectory or largest isoflux locus $\partial\bar{\Lambda}$ by computing the intersection torque. If $|T| < T_i$, the drive system is operated with $i_{dq}^{\star} \in$ MTPA and if $T_i \le |T| < T_m$, the drive system is operated with $i_{dq}^{\star} \in \partial\bar{\Lambda}$. Otherwise, the torque reference $|T| \ge T_m$ corresponds or exceeds the maximum torque, and the drive system applies the maximum torque. It is observed that the maximum and intersection torque can be computed independent from each other. Therefore, step two and three can be easily implemented using parallel computation if the control hardware supports it.

In the fourth step, the optimal current $i_{dq}^{\star} \in$ MTPA, i.e., $i_{dq}^{\star} \in \partial\bar{\Lambda}$, which produce the reference torque T are computed. The optimal states can be computed either directly (solving a quartic equation) or using numerical methods. The equations are given in the Appendixes. The resulting $i_{dq}^{\star}$ are shown in Fig. 6, where the trajectory A refers to base mode (constant torque mode) and the trajectories B and C refer to operation in field weakening.

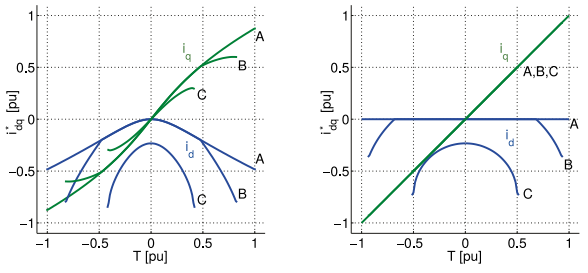

Fig. 6. Optimal current $i^{\star}_{dq}$ as a function of $T \in [-T_m, T_m]$ at different speeds ω. (a) $L_d < L_q$; $\chi_m = \infty$. (b) $L_d = L_q$; $\chi_m = \infty$.

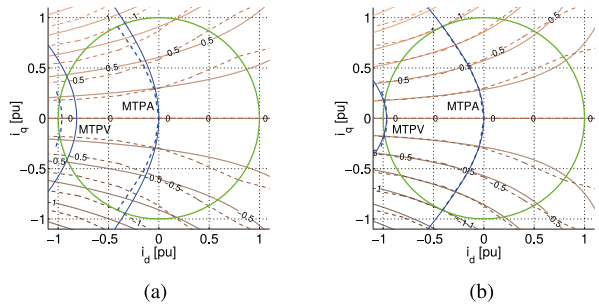

Fig. 7. Comparison of the modeled (solid) and measured (dashed) PMSM characteristics. (a) Rated parameters. (b) Optimized parameters.

VIII. Local Optimization of the Torque Model

The presented procedure relies on a sufficiently accurate PMSM torque model and its main characteristics (isotorque locus, MTPA and MTPV trajectory). However, using the rated parameters[1] of an electrical machines can provide mediocre results, i.e., a rough approximation of the real behavior. An example is shown in Fig. 7(a), where the modeled characteristics are compared to the measured ones.

In this section, an approach is proposed to improve the model consistency based on known operation points. The model does not need to describe the machine globally but has to capture the local machine behavior (the area on the left-hand side of the MTPA trajectory and inside the set $\mathcal{I}$). Thus, the parameters can be optimized to increase the model correspondence in this region. The parameters can be settled with respect to the rated operation point with the rated current $i_r = [i_{dr}, i_{qr}]'$ and the rated flux $\lambda_r = [\lambda_{dr}, \lambda_{qr}]'$ producing the torque T_r using the equations:

1) the torque equation $3/2(\psi + (L_d - L_q)i_{dr})i_{qr} - T_r/p$;
2) the MTPA trajectory $\psi i_d + (L_d - L_q)(i_{dr}^2 - i_{qr}^2) = 0$;
3) the rated current-flux relation $\mathbf{L}i_r + \psi_{dq} = \lambda_r$.

The high-speed behavior of a PMSM depends whether a machine has infinite ($\chi_m = \infty$) or finite ($\chi_m < \infty$) maximum speed and so does the parameter assessment procedure for the torque plane on the left-hand side of the MTPA trajectory. For machines with $\chi_m = \infty$, the location of the MTPV trajectory needs to be settled. This can be achieved using the demagnetization current $i_c = [i_{\mathrm{dc}}, 0]'$ that yields the short-circuit current-flux relation $\mathbf{L}i_c + \psi_{dq} = 0$. For machines with $\chi_m < \infty$, the high-speed behavior can be settled using the rated power operation point $i_p = [i_{dp}, 0]'$ and $\lambda_p = [\lambda_{dp}, 0]'$, where the machine achieves its maximum speed that yields the rated power current-flux relation $\mathbf{L}i_p + \psi_{dq} = \lambda_p$. Combining the equations, the following overdetermined equation system is achieved for a PMSM with $\chi_m = \infty$:

$$\begin{bmatrix} \frac{3}{2}i_{qr} & \frac{3}{2}i_{dr}i_{qr} & -\frac{3}{2}i_{dr}i_{qr} & -T_r \\ i_d & i_{dr}^2 - i_{qr}^2 & i_{qr}^2 - i_{dr}^2 & \\ 1 & i_{dr} & & \\ & & i_{qr} & \\ 1 & i_{\mathrm{dc}} & & \end{bmatrix} \begin{bmatrix} \psi \\ L_d \\ L_q \\ 1/p \end{bmatrix} = \begin{bmatrix} 0 \\ 0 \\ \lambda_{dr} \\ \lambda_{qr} \\ 0 \end{bmatrix} \tag{19}$$

where the last row needs to be replaced for a PMSM with $\chi_m < \infty$. The system can be written compactly as $\mathbf{M}\rho = K$ with the least-squares solution $\rho = \mathbf{M}^{\dagger}K$, which tends to give the best results when the equations are normalized (p.u.). An example of an optimized model computed with this approach is shown in Fig. 7(b).

This approach aims to improve the model locally where the machine is operated. It is capable of delivering models that are locally exact to measurement precision. The result is a typically good approximation based on (4) but may not characterize well PMSM with arbitrarily large saturation and cross saturation. The motor parameters can also vary with temperature (typically the PM flux). If the variation is significant, a low- and high-temperature-optimized model can be produced such that the parameters can be computed via interpolation online. However, the MTPA, i.e., MTPV, is a flat optimum such that operation close but not on the trajectory does not increase the current magnitude, i.e., decrease the maximum torque in reduced power operation, by a significant amount.

Applying the torque T may produce a higher flux magnitude $\|\lambda_{dq}\|$ than predicted by the model. Thus, it is good practice to use the voltage safety factor $\rho_v \in (0, 1)$ as explained in Section III. The modeled intersection and maximum torque

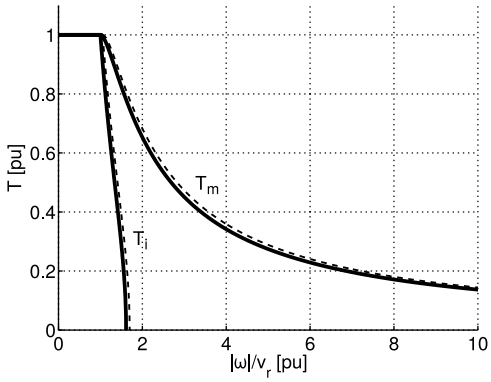

Fig. 8. Torque characteristics T_i and T_m : model with safety factor (solid) and measure (dashed).

[1]The *rated* L_d and L_q parameters define the slope of the d- and q-axis flux in the origin, respectively, where the current on the other axis is set to zero. The *rated* ψ defines the offset of the d-axis flux in the origin. These rated parameters provide the linear approximations shown in Fig. 2.

TABLE II
DRIVE SYSTEM PARAMETERS

Inverter and Control	
Type	2L-VSI
Grid interface	diode bridge
DC-link voltage v_c	120 V
Voltage safety factor ρ_v	0.95
Embedded control platform	dSpace 1104
Sampling time T_s	200μs
Electric Machine	
Type	IPMSM
Rated current I_s	10 A
Rated torque T_r	8.0 Nm
Rated flux λ_r	142.5 mWb
Inductance (d-axis) L_d	9.1 mH
Inductance (q-axis) L_q	14.6 mH
Stator resistance R_s	636 mΩ
PM rotor flux ψ	88.3 mWb
Pole pairs p (model, physical)	5.3, 5
Shaft friction B	$6.4 \cdot 10^{-3}$ Nm s
Shaft inertia J	$5.0 \cdot 10^{-3}$ kgm^2
Norm. rated speed $\chi_r = \omega_r / \bar{v}_r = 1/\lambda_r$	7.0 Wb^{-1}
Norm. rated power speed $\chi_p = \omega_p / \bar{v}_r$	45.3 Wb^{-1}
Norm. intersection speed $\chi_i = \omega_i / \bar{v}_r = 1/\psi$	11.3 Wb^{-1}
Norm. max. speed χ_m	∞

characteristics (with safety factor $\rho_v = 0.95$) are compared to the measured ones in Fig. 8. The safety factor essentially decreases the available voltage. Thus, the speed limit of the rated torque and rated power region shifts to the left (by a limited amount), and the intersection and maximum torque is reduced (by a limited amount above rated speed). This section is concluded by observing that (19) issues parameters, which optimize the correspondence of the modeled and real torque plane. However, they may be suboptimal for other purposes. For example, the resulting number pole pairs p is a nonnegative real number (not an integer) in general.

IX. EVALUATION

The reference generation procedure is evaluated on an SiL platform, where the electrical machine is simulated by MATLAB/Simulink, and an experimental test bench with the (optimized) parameters shown in Table II. The generated current reference is applied to the system by a state (current) controller. Three different types of controllers have been evaluated: a nonlinear controller (NLC), convex control set (CCS) model-predictive control (MPC), and finite control set (FCS) MPC [19]. NLC and CCS-MPC use space vector modulation. FCS-MPC actuates switching states directly without modulation scheme. All controllers are executed at the same sampling frequency.

A dSpace 1104 is used as control hardware on the experimental test bench. It uses internally a 250-MHz PowerPC for computation and a 20-MHz TI TMS320F240 for communication (A/D, PWM). Due to the (dSpace) communication between PowerPC and TMS320F240, only 50% of a sampling period is available to compute the control code. On the experimental test bench, the minimum, mean, and maximum execution time of the reference generation procedure is 34.7, 46.5, and 54.2 μs, respectively. The variation is caused since some paths of the reference generation procedure (see Fig. 5) are significantly simpler to compute than others.

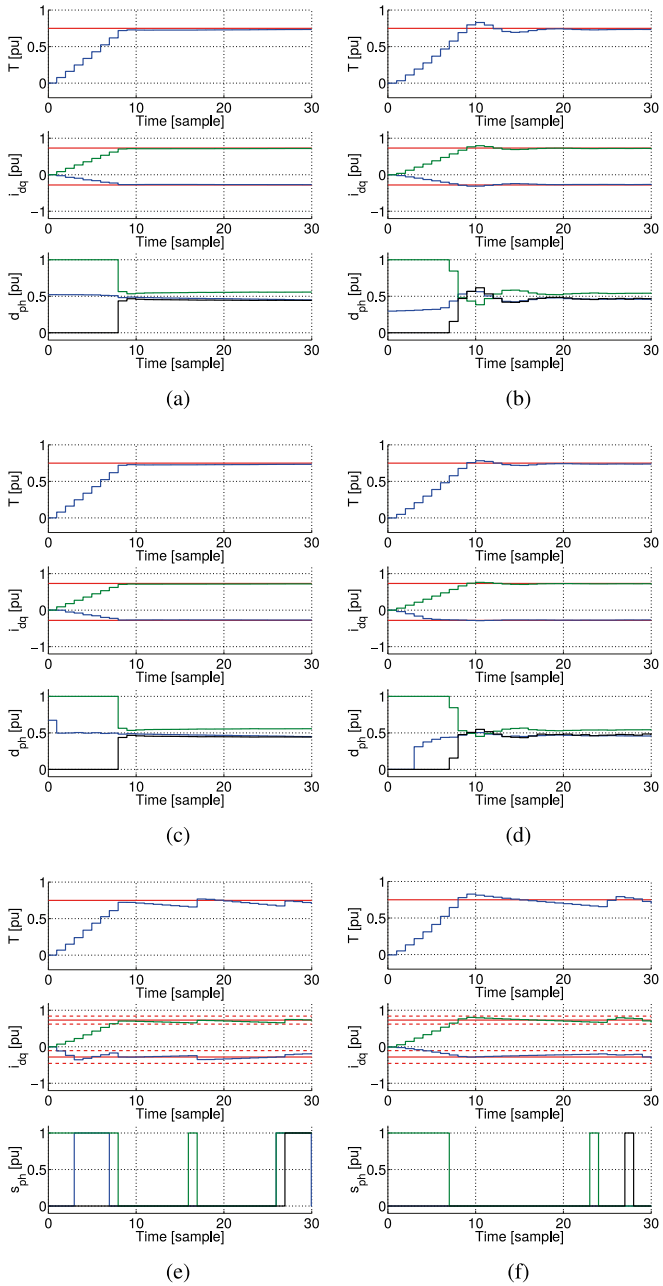

Fig. 9. Torque step from 0 to 0.75 p.u. at standstill ($d_{\rm ph}$ is the three-phase duty cycle and $s_{\rm ph}$ is the discrete switching function). (a) NLC simulation. (b) NLC experimentation. (c) CCS-MPC simulation. (d) CCS-MPC experimentation. (e) FCS-MPC simulation. (f) FCS-MPC experimentation.

The behavior of the reference generation procedure is explained on a torque step at standstill. At $t = 0$ s, a torque step

[2]A later optimization of the c-code has reduced the execution times by approximately 50% on the SiL platform but was not evaluated on the experimental test bench.

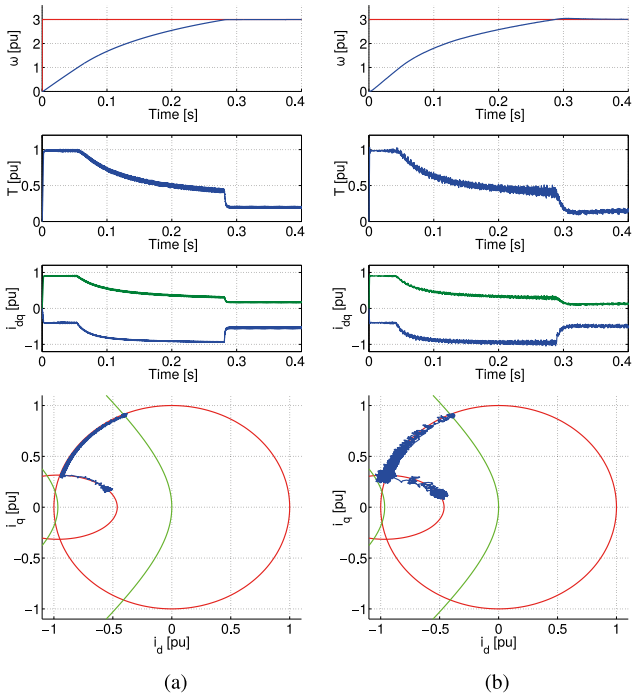

Fig. 10. Speed step form standstill to 3 p.u. using NLC. (a) NLC simulation. (b) NLC experimentation.

from 0 to 0.75 p.u. is applied. The reference generation procedure provides the optimal current references instantaneously. The d and q current reference values are applied to the inner current controller, which reduces the (current) control error applying a voltage to the machine terminals. It is noted that the trajectory of the states (currents) toward their reference depends on the current controller. The results are shown in Fig. 9.

A speed reference step from standstill to 3 p.u. is applied to the machine using an antiwindup proportional-integral speed controller. Since the reference step is large, the speed loop saturates, and the maximum available torque is applied approximately until the speed reference is reached. At low speed, the maximum torque and acceleration are constant. The current-producing maximum torque lies on the intersection of the MTPA and the isocurrent locus. Increasing the speed beyond rated speed, this operation point is not available anymore due to the voltage limit. Thus, the current moves along the isocurrent locus until the reference speed is achieved. Then, the current moves along the isoflux locus to the operation point which provides the torque to maintain the machine at reference speed. The results are presented in Figs. 10 and 11.

To check the convergence to the optimal operation points, different load torques are applied such that the machine provides a constant torque T at different speeds ω. The cases:

1) $\omega = 1.0\,\text{p.u.}$ with $T = \{0\,\text{p.u.}, 0.25\,\text{p.u.}, 0.5\,\text{p.u.}, 0.75\,\text{p.u.}\}$;
2) $\omega = 2.0\,\text{p.u.}$ with $T = \{0\,\text{p.u.}, 0.25\,\text{p.u.}, 0.5\,\text{p.u.}\}$;
3) $\omega = 3.0\,\text{p.u.}$ with $T = \{0\,\text{p.u.}, 0.25\,\text{p.u.}\}$

are evaluated, and the simulation and experimental results are shown in Fig. 12. Ideally, steady-state operation with given

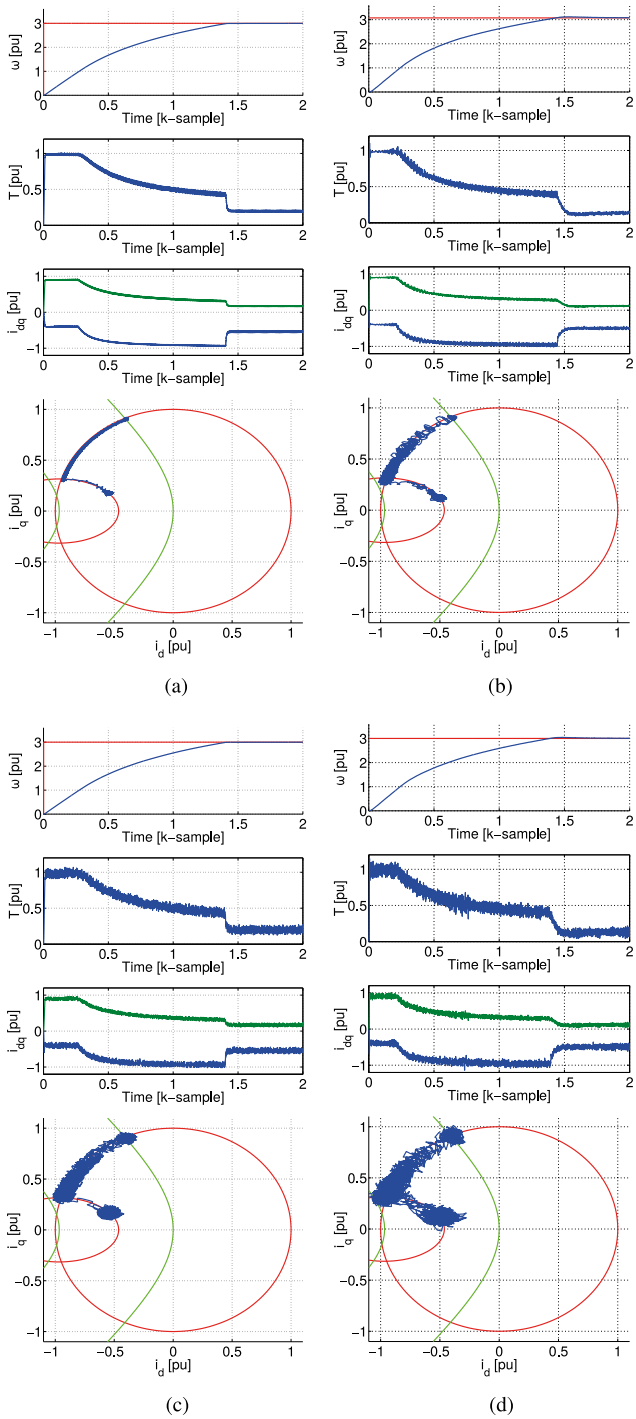

Fig. 11. Speed step form standstill to 3 p.u. using MPC. (a) CCS-MPC simulation. (b) CCS-MPC experimentation. (c) FCS-MPC simulation. (d) FCS-MPC experimentation.

conditions (torque, speed) would lead to a single point on the state plane. In practice, the states stay in the neighborhood of this point due to power converter switching, measurement noise, etc. The results show that the drive system applies states according to the reference generation procedure. The controller operates on the MTPA trajectory at $\omega = 1.0\,\text{p.u.}$ At $\omega = 2.0\,\text{p.u.}$ and $\omega = 3.0\,\text{p.u.}$, the system operates on the isoflux locus, which is defined by the speed ω.

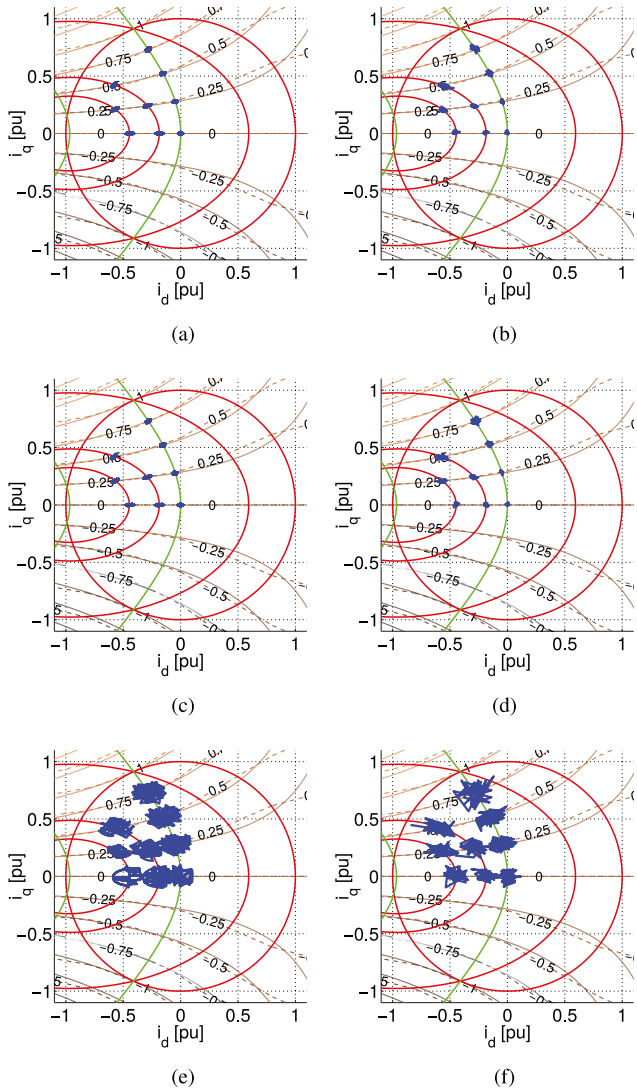

Fig. 12. Steady-state operation points. (a) NLC simulation. (b) NLC experimentation. (c) CCS-MPC simulation. (d) CCS-MPC experimentation. (e) FCS-MPC simulation. (f) FCS-MPC experimentation.

X. Conclusion

The present research proposes an approach to compute an optimal current reference vector from a torque reference value. Optimality is achieved with respect to the constrained MTPA criterion that is a generalization of MTPA tracking. Since the optimization problem is difficult to solve directly, the maximum and intersection torque subproblems are identified. These concepts are used to define an algorithm that provides the optimal current reference vector and is sufficiently efficient for online implementation. The method supports a variety of state (current) controllers with/without PWM, SPM and IPM machines with saliency and reverse saliency, and a variable dc-link voltage. To improve the correspondence between the model and the real machine, an approach is proposed to optimize the machine parameters locally with respect to important operation points. The concepts are developed on an SiL platform and evaluated on an experimental test bench with good results. In further work, the proposed procedure will be combined with high-performance current controllers. In particular, the combination with model-predictive current control yields a novel high-performance torque control strategy.

Appendix A

A. Trajectories and Loci

In this section, the trajectories and loci are defined using either the current or flux space. They can be transformed between the spaces using (4), i.e.,

$$\lambda_d = L_d i_d + \psi \quad \text{and} \quad \lambda_q = L_q i_q. \tag{20}$$

The isocurrent locus is defined by an ellipsis (circle) in the current space

$$\frac{i_d^2}{I_r^2} + \frac{i_q^2}{I_r^2} = 1 \tag{21}$$

and the isoflux locus in defined by an ellipsis (circle) in the flux space

$$\frac{\lambda_d^2}{\left(\bar{v}_r/|\omega|\right)^2} + \frac{\lambda_q^2}{\left(\bar{v}_r/|\omega|\right)^2} = 1. \tag{22}$$

The MTPA trajectory is defined by a hyperbola in the current plane [3], [19]

$$\frac{\left(i_d + \frac{\psi}{2(L_d - L_q)}\right)^2}{\left(\frac{\psi}{2(L_d - L_q)}\right)^2} - \frac{i_q^2}{\left(\frac{\psi}{2(L_d - L_q)}\right)^2} = 1 \tag{23}$$

for the IPM and $i_d = 0A$ for the SPM. The MTPV trajectory is defined by a hyperbola in the flux plane [7], [19]

$$\frac{\left(\lambda_d + \frac{L_q \psi}{2(L_d - L_q)}\right)^2}{\left(\frac{L_q \psi}{2(L_d - L_q)}\right)^2} - \frac{\lambda_q^2}{\left(\frac{L_q \psi}{2(L_d - L_q)}\right)^2} = 1 \tag{24}$$

for the IPM and $\lambda_d = 0Wb$ for the SPM. Both, (23) and (24) define two trajectories each. The hyperbola on the left, i.e., right, hand side is the correct solution for a machine with $L_d < L_q$, i.e., $L_d > L_q$, respectively.

The MTPV trajectory crosses the d-axis in $\lambda_d = 0Wb$, i.e., $i_d = -\psi/L_d$. Observing Fig. 4, it is immediately clear that for a SPM and IPM with $L_d < L_q$, an intersection of the MTPV and isocurrent exists iff $\psi/L_d \leq I_r$. However, this result is less clear for machines with $L_d > L_q$ as shown in Fig. 13. One could suspect the existence of a case where the MTPV trajectory intersects the isocurrent locus in Fig. 13(c).

Proposition 1: The MTPV trajectory (24) never penetrates the feasible current space $\|i_{dq}\| \leq I_r$ if $\psi/L_d > I_r$.

Proof: This result is well known for SPM and IPM with $L_d < L_q$, where no intersection of the MTPV trajectory and isocurrent locus exists if $\psi/L_d > I_r$.

Let $\psi/L_d > I_r$ and $L_d > L_q$, then the MTPV trajectory needs to intersect the isocurrent locus twice along the d axis to penetrate the feasible current space (two λ_d defining an entry and exit point; each associated with a $\pm\lambda_d$ value). Since the feasible currents ($i_{dq} \in \mathcal{I}$) lie entirely on the positive halfplane

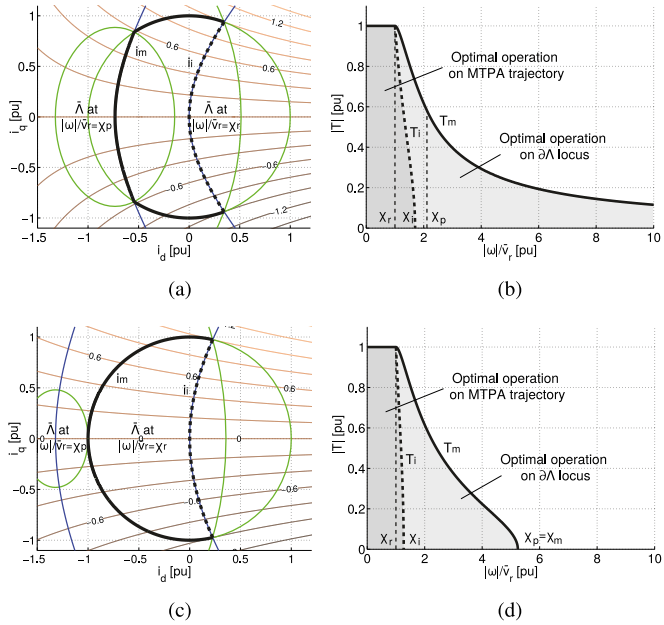

Fig. 13. Maximum and intersection torque characteristic of a reverse saliency machine ($L_d > L_q$). (a) and (b) Infinite maximum speed $\chi_m = \infty$. (c) and (d) Finite maximum speed $\chi_m < \infty$. (a) Current space. (b) Torque versus normalized speed. (c) Current space. (d) Torque versus normalized speed.

$\lambda_d > 0Wb$ (for $\psi/L_d > I_r$), the intersection between MTPV and isocurrent needs to have two solutions on $\lambda_d > 0Wb$.

The d axis components of the intersections of the MTPV trajectory and the isocurrent locus are defined by (30)

$$\lambda_d = -b \pm \sqrt{b^2 + a} \tag{25}$$

with

$$b = \frac{L_q \psi}{2(L_d - L_q)} \frac{(L_d - L_q)^2 + L_q^2}{L_d^2 + L_q^2)} > 0 \tag{26}$$

Hence the d axis component of the intersection has at most two real roots; one is located on the left hand side and the other is located on the right hand side of the asymptote $\lambda_d = -b$. Since the asymptote $\lambda_d = -b$ belongs to the negative halfplane $\lambda_d < 0Wb$ (for $\psi/L_d > I_r$), one root is always negative. Thus, the MTPV trajectory has at maximum one intersection with the isocurrent locus. ■

The above result is sufficient such that the proposed analysis and method (see Fig. 5) is suitable for machines with $L_d > L_q$.

APPENDIX B

A. Computation

The maximum and intersection torque are obtained intersecting the relevant trajectories and loci defined in Fig. 5. Each intersection is obtained substituting the relevant equations that yield second-order polynomials and can be solved analytically. The intersection of the *isocurrent locus and MTPA trajectory* is obtained at i_d given by

$$2L_\Delta i_d^2 + \psi i_d - L_\Delta I_r^2 = 0 \tag{27}$$

where $L_\Delta \overset{\text{def}}{=} L_d - L_q$. The q-axis component is recovered substituting i_d into (21) or (23). The intersection of the *isoflux locus and MTPV trajectory* is obtained at λ_d given by

$$2L_\Delta \lambda_d^2 + L_q \psi \lambda_d - L_\Delta \bar{\lambda}_r^2 = 0 \tag{28}$$

where $\bar{\lambda}_r \overset{\text{def}}{=} \bar{v}_r/|\omega|$. The q-axis component is recovered substituting λ_d into (22) or (24). The intersection of the *isoflux locus and MTPA trajectory* is obtained at i_d given by

$$L_\Delta (L_d^2 + L_q^2) i_d^2 + \psi (L_d^2 + L_\Delta^2) i_d + L_\Delta (\psi^2 - \bar{\lambda}_r^2) = 0. \tag{29}$$

The q-axis component is recovered substituting i_d into (22) or (23). The intersection of the *isocurrent locus and MTPV trajectory* is obtained at λ_d given by

$$\begin{aligned} &L_\Delta (L_d^2 + L_q^2) \lambda_d^2 + L_q \psi (L_q^2 + L_\Delta^2) \lambda_d \\ &+ L_q^2 L_\Delta \left(\psi^2 - L_d^2 I_r^2\right) = 0. \end{aligned} \tag{30}$$

The q-axis component is recovered substituting λ_d into (21) or (24). The intersection of the *isocurrent locus and isoflux locus* is obtained at i_d given by

$$(L_d^2 - L_q^2) i_d^2 + 2L_d \psi i_d + \psi^2 - \bar{\lambda}_r^2 + L_q^2 I_r^2 = 0. \tag{31}$$

The q-axis component is recovered substituting i_d into (21) or (22).

The states on the MTPA trajectory, i.e., isoflux locus, which produce a given torque, are obtained substituting (22), i.e., (23), into the torque (6). This yields fourth-order polynomials that can be solved analytically with the Ferrari's method. Solving the fourth-order polynomial (one per iteration) is the most demanding step of the reference generation procedure in terms of computation effort. Given a torque T, the states on the MTPA trajectory that produce T are defined by i_d given by

$$L_\Delta^3 i_d^4 + 3L_\Delta^2 \psi i_d^3 + 3L_\Delta \psi^2 i_d^2 + \psi^3 i_d - L_\Delta \bar{T}^2 = 0 \tag{32}$$

where $\bar{T} = T/(3/2p)$. The q-axis component is recovered substituting i_d into (23). Given a torque T, the states on the isoflux locus that produce T are defined by i_d given by

$$\begin{aligned} &-L_d^2 L_\Delta^2 i_d^4 - 2L_d \psi L_\Delta (2L_d - L_q) i_d^3 \\ &+ (\bar{\lambda}_r^2 L_\Delta^2 - \psi^2 (6L_d^2 - 6L_d L_q + L_q)) i_d^2 \\ &+ 2\psi (\bar{\lambda}_r^2 L_\Delta - \psi^2 (2L_d - L_q)) i_d \\ &+ \psi^2 (\bar{\lambda}_r^2 - \psi^2) - L_q^2 \bar{T}^2 = 0. \end{aligned} \tag{33}$$

The q-axis component is recovered substituting i_d into (22).

REFERENCES

[1] N. Bianchi and S. Bolognani, "Parameters and volt-ampere ratings of a synchronous motor drive for flux-weakening applications," *IEEE Trans. Power Electron.*, vol. 12, no. 5, pp. 895–903, Sep. 1997.

[2] A. Consoli, G. Scelba, G. Scarcella, and M. Cacciato, "An effective energy-saving scalar control for industrial IPMSM drives," *IEEE Trans. Ind. Electron.*, vol. 60, no. 9, pp. 3658–3669, Sep. 2013.

[3] M. Preindl and S. Bolognani, "Model predictive direct torque control with finite control set for PMSM drive systems, part 1: Maximum torque per ampere operation," *IEEE Trans. Ind. Informat.*, vol. 9, no. 2, pp. 1912–1921, May 2013.

[4] J. Beerten, J. Verveckken, and J. Driesen, "Predictive direct torque control for flux and torque ripple reduction," *IEEE Trans. Ind. Appl.*, vol. 57, no. 1, pp. 404–412, Jan. 2010.

[5] M. Preindl, E. Schaltz, and P. Thøgersen, "Switching frequency reduction using model predictive direct current control for high power voltage source inverters," *IEEE Trans. Ind. Electron.*, vol. 58, no. 7, pp. 2826–2835, Jul. 2011.
[6] K. Kamiev, J. Montonen, M. Ragavendra, J. Pyrhonen, J. Tapia, and M. Niemela, "Design principles of permanent magnet synchronous machines for parallel hybrid or traction applications," *IEEE Trans. Ind. Electron.*, vol. 60, no. 11, pp. 4881–4890, Nov. 2013.
[7] M. Preindl and S. Bolognani, "Model predictive direct torque control with finite control set for PMSM drive systems, part 2: Field weakening operation," *IEEE Trans. Ind. Informat.*, vol. 9, no. 2, pp. 648–657, May 2013.
[8] Y. Inoue, S. Morimoto, and M. Sanada, "Comparative study of PMSM drive systems based on current control and direct torque control in flux-weakening control region," *IEEE Trans. Ind. Appl.*, vol. 48, no. 6, pp. 2382–2389, Nov./Dec. 2012.
[9] S. Bolognani, S. Calligaro, and R. Petrella, "Adaptive flux-weakening controller for interior permanent magnet synchronous motor drives," *IEEE J. Emerg. Sel. Topics Power Electron.*, vol. 2, no. 2, pp. 236–248, Jun. 2014.
[10] S. Morimoto, Y. Takeda, T. Hirasa, and K. Taniguchi, "Expansion of operating limits for permanent magnet motor by current vector control considering inverter capacity," *IEEE Trans. Ind. Appl.*, vol. 26, no. 5, pp. 866–871, Sep./Oct. 1990.
[11] S.-Y. Jung, J. Hong, and K. Nam, "Current minimizing torque control of the IPMSM using Ferrari's method," *IEEE Trans. Power Electron.*, vol. 28, no. 12, pp. 5603–5617, Dec. 2013.
[12] M. Preindl and E. Schaltz, "Sensorless model predictive direct current control using novel second-order PLL observer for PMSM drive systems," *IEEE Trans. Ind. Electron.*, vol. 58, no. 9, pp. 4087–4095, Sep. 2011.
[13] T. Miyajima, H. Fujimoto, and M. Fujitsuna, "A precise model-based design of voltage phase controller for IPMSM," *IEEE Trans. Power Electron.*, vol. 28, no. 12, pp. 5655–5664, Dec. 2013.
[14] M. Kunter, T. Schoenen, W. Hoffmann, and R. De Doncker, "IPMSM control regime for a hybrid-electric vehicle application," in *Proc. Emobility—Elect. Power Train*, 2010, pp. 1–5.
[15] J. Lemmens, P. Vanassche, and J. Driesen, "Pmsm drive current and voltage limiting as a constraint optimal control problem," *IEEE J. Emerg. Sel. Topics Power Electron.*, 2014, doi:10.1109/JESTPE.2014.2321111.
[16] K. Hoang, J. Wang, M. Cyriacks, A. Melkonyan, and K. Kriegel, "Feedforward torque control of interior permanent magnet brushless AC drive for traction applications," in *Proc. Int. Electric Mach. Drives Conf.*, 2013, pp. 152–159.
[17] C. Mademlis and V. Agelidis, "A high-performance vector controlled interior PM synchronous motor drive with extended speed range capability," in *Proc. Annu. Conf. IEEE Ind. Electron. Soc.*, 2001, pp. 1475–1482.
[18] L. Montejano, "Some results about Minkowski addition and difference," *Mathematika*, vol. 43, pp. 265–273, 1996.
[19] M. Preindl, "Novel model predictive control of a PM synchronous motor drive," Ph.D. dissertation, Dept. Ind. Eng., Univ. Padova, Padova, Italy, 2014.
[20] S. Morimoto, M. Sanada, and Y. Takeda, "Effects and compensation of magnetic saturation in flux-weakening controlled permanent magnet synchronous motor drives," *IEEE Trans. Ind. Appl.*, vol. 30, no. 6, pp. 1632–1637, Nov./Dec. 1994.
[21] Y. Chen, Z. Zhu, and D. Howe, "Influence of inaccuracies in machine parameters on field-weakening performance of PM brushless AC drives," in *Proc. Int. Electric Mach. Drives Conf.*, 1999, pp. 691–693.
[22] Y. F. Shi, Z. Zhu, Y. Chen, and D. Howe, "Influence of winding resistance on flux-weakening performance of a permanent magnet brushless AC drive," in *Proc. Int. Conf. Power Electron., Mach. Drives*, 2002, pp. 392–397.
[23] T. Schoenen, M. Kunter, M. Hennen, and R. De Doncker, "Advantages of a variable DC-link voltage by using a DC-DC converter in hybrid-electric vehicles," in *Proc. Veh. Power Propul. Conf.*, 2010, pp. 1–5.
[24] M. Preindl and D. Bagnara, "Wind turbine for generating electric energy," Patent WO2 013 001 496, 2013.
[25] R. H. Park, "Two-reaction theory of synchronous machines generalized method of analysis—part I," *Trans. Am. Inst. Electr. Eng.*, vol. 48, pp. 716–727, 1929.
[26] F. Parasliti and P. Poffet, "A model for saturation effects in high-field permanent magnet synchronous motors," *IEEE Trans. Energy Convers.*, vol. 4, no. 3, pp. 487–494, Sep. 1989.
[27] C. Mademlis and V. Agelidis, "On considering magnetic saturation with maximum torque per current control in interior permanent magnet synchronous motor drives," *IEEE Trans. Energy Convers.*, vol. 16, no. 3, pp. 246–252, Sep. 2001.
[28] B. Stumberger, G. Stumberger, D. Dolinar, A. Hamler, and M. Trlep, "Evaluation of saturation and cross-magnetization effects in interior permanent-magnet synchronous motor," *IEEE Trans. Ind. Appl.*, vol. 39, no. 5, pp. 1264–1271, Sep./Oct. 2003.
[29] N. Bianchi and T. M. Jahns, *Design, Analysis, and Control of Interior PM Synchronous Machines*. Padua, Italy, Cleup, 2006.
[30] N. Bianchi, S. Bolognani, and B. Ruzojcic, "Design of a 1000 HP permanent magnet synchronous motor for ship propulsion," in *Proc. Eur. Conf. Power Electron. Appl.*, 2009, pp. 1–8.
[31] M. Barcaro, "Design and analysis of interior permanent magnet synchronous machines for electric vehicles," Ph.D. dissertation, Dept. Electr. Eng., Univ. Padova, Padova, Italy, 2011. [Online]. Available: http://paduaresearch.cab.unipd.it/3497/
[32] D. White and H. Woodson, *Electromechanical Energy Conversion*. New York, NY, USA: Wiley, 1959.
[33] M. Preindl and S. Bolognani, "Model predictive direct speed control with finite control set of PMSM drive systems," *IEEE Trans. Power Electron.*, vol. 28, no. 2, pp. 1007–1015, Feb. 2013.
[34] S. Boyd and L. Vandenberghe, *Convex Optimization*. Cambridge, U.K.: Cambridge Univ. Press, 2004. [Online]. Available: http://www.stanford.edu/ boyd/cvxbook/
[35] M. Zordan, P. Vas, M. Rashed, S. Bolognani, and M. Zigliotto, "Field-weakening in high-performance PMSM drives: A comparative analysis," in *Proc. Ind. Appl. Conf.*, 2000, pp. 1718–1724.
[36] S. Bolognani, S. Calligaro, R. Petrella, and F. Pogni, "Flux-weakening in IPM motor drives: Comparison of state-of-art algorithms and a novel proposal for controller design," in *Proc. Eur. Conf. Power Electron. Appl.*, 2011, pp. 1–11.

Matthias Preindl (S'13) received the Ph.D. degree in energy engineering from the Doctoral School of Industrial Engineering, University of Padua, Padua, Italy, in 2014, the M.Sc. degree in electrical engineering and information technology from ETH Zurich, Zurich, Switzerland, in 2010, and the B.Sc. degree in electrical engineering from the University of Padua in 2008.

He is a Postdoctoral Research Associate at the McMaster Institute for Automotive Research and Technology, McMaster University, Canada. He was a Visiting Scholar and Visiting Student at the University of California, Berkeley, CA, USA, and Aalborg University, Aalborg, Denmark, respectively. Also, he was a trainee at the National Research Council (CNR), Italy. From 2010 to 2012, he was with Leitwind AG, Italy, where he was an R&D Engineer in power electronic and drives. He obtained several honors including merit scholarships, a price for outstanding achievements during his studies, and a best presentation award. He is involved in design and control of power electronic and drive systems with primary focus on renewable energy power plants and innovative transportation systems.

Silverio Bolognani (M'98) received the Laurea degree in electrical engineering from the University of Padua, Padua, Italy, in 1976.

In 1976, he joined the Department of Electrical Engineering, University of Padova. He then started the Electrical Drives Laboratory, where a variety of research work on brushless and induction motor drives is carried out in the frame of European and the national research projects. He is a Full Professor of electrical converters, machines, and drives in the same department. His research interests include advanced control techniques for motor drives and motion control and design of ac electrical motors for variable-speed applications. He is an author of more than 200 papers on electrical machines and drives and is the holder of three patents.

Dr. Bolognani has been serving international conferences as a Member of the steering or technical committees, as well as an invited speaker. He is currently the Chairman of the IEEE North Italy IEEE Industry Applications/Industrial Electronics/Power Electronics Societies Joint Chapter.